A Fast-Conducting, Stochastic Integrative Mode for Neocortical Neurons *In Vivo*

Michael Rudolph and Alain Destexhe

Integrative and Computational Neuroscience Unit, Centre National de la Recherche Scientifique, 91198 Gif-sur-Yvette, France

During activated states, neocortical neurons receive intense synaptic background activity that induces large-amplitude membrane potential fluctuations and a strong conductance in the membrane. However, little is known about the integrative properties of neurons during such high-conductance states. Here we investigated the integrative properties of neocortical pyramidal neurons under *in vivo* conditions simulated by computational models. We show that the presence of high-conductance fluctuations induces a stochastic state in which active dendrites are fast conducting and have a different dynamics of initiation and forward-propagation of Na^+-dependent spikes. Synaptic efficacy, quantified as the probability that a synaptic input specifically evokes a somatic spike, was approximately independent of the dendritic location of the synapse. Synaptic inputs evoked precisely timed responses (milliseconds), which also showed a reduced location dependence. This scheme was found to apply to a broad range of kinetics and density distributions of voltage-dependent conductances, as well as to different dendritic morphologies. Synaptic efficacies were, however, modulable by the balance of excitation and inhibition in background activity, for all synapses at once. Thus, models predict that the intense synaptic activity *in vivo* can confer advantageous computational properties to neocortical neurons: they can be set to an integrative mode that is stochastic, fast conducting, and optimized to process synaptic inputs at high temporal resolution independently of their position in the dendrites. Some of these predictions can be tested experimentally.

Key words: computational models; random synaptic inputs; noise; high-conductance state; synaptic integration; dendritic democracy

Introduction

How the extended dendritic trees of central neurons integrate synaptic inputs is a problem that must be solved to understand how information is processed or coded in neurons (Yuste and Tank, 1996; Magee, 2000; Stuart et al., 2000). The high precision of patch-clamp and whole-cell recordings, together with the possibility of a fine control of synaptic inputs *in vitro*, has allowed significant advances in this field (Cash and Yuste, 1999; Pouille and Scanziani, 2001; Williams and Stuart, 2002). Cortical neurons possess several types of voltage- and calcium-dependent ion channels in their dendrites (Llinás, 1975; Johnston et al., 1996; Yuste and Tank, 1996; Stuart et al., 2000), which may significantly affect the impact of synaptic inputs at the level of the soma (Crill and Schwindt, 1995; Stuart and Sakmann, 1995; Williams and Stuart, 2000a; Berger et al., 2001), and generate calcium- and sodium-dependent spikes in dendrites (Spencer and Kandel, 1961; Wong et al., 1979; Benardo et al., 1982; Regehr et al., 1993; Andreasen and Lambert, 1995). Pyramidal neurons can generate action potentials (APs) that are initiated in the axon and propagate backward in the dendritic tree (Stuart and Sakmann, 1994; Stuart et al., 1997b; Häusser et al., 2000) or APs initiated in dendrites that propagate forward to the soma (Schwindt and Crill, 1997, 1998; Stuart et al., 1997a; Golding and Spruston, 1998; Williams and Stuart, 2002).

However, how neocortical neurons integrate synaptic inputs during activated states in the intact brain is a question yet unanswered, mainly because of the technical difficulty of controlling identified subsets of synaptic inputs *in vivo*. Here we address this problem by using computational models of morphologically reconstructed neocortical pyramidal neurons with active dendrites. *In vivo* conditions were simulated by random excitatory and inhibitory synaptic inputs in soma and dendrites based on constraining the model to intracellular recordings *in vivo* (Destexhe and Paré, 1999). In agreement with previous theoretical (Barrett, 1975; Holmes and Woody, 1989; Bernander et al., 1991; Rapp et al., 1992) and experimental (Borg-Graham et al., 1998; Paré et al., 1998b) studies, this approach revealed that background activity *in vivo* is responsible for a major tonic increase of conductance compared with quiescent states.

Thus, *in vitro* measurements have demonstrated the importance of active dendritic currents to capture the subthreshold and superthreshold dynamics of dendrites. On the other hand, *in vivo* studies demonstrated that cortical neurons are subject to a high-conductance fluctuating activity during activated states of the brain. Here we use models based on both *in vitro* and *in vivo* measurements in an attempt to characterize the effect of these high-conductance fluctuations on the integrative properties of neocortical pyramidal neurons.

Materials and Methods

Computational models of morphologically reconstructed neocortical pyramidal neurons were simulated using NEURON (Hines and Carnevale, 1997) and were constrained by experimental data obtained from *in vitro* and *in vivo* preparations, as detailed below.

Dendritic morphologies. Dendritic morphologies were obtained from three-dimensional reconstructions of four pyramidal cells (one from layer II–III, two from layer V, and one from layer VI) obtained from cat cortex (Douglas et al., 1991; Contreras et al., 1997). The cellular geometries were corrected for spines assuming that spines represent ~45% of the dendritic membrane area (DeFelipe and Farinas, 1992).

Passive properties. Passive properties (leak conductance, reversal potential, and axial resistance) were obtained by fitting the model to passive responses obtained intracellularly after application of tetrodotoxin and synaptic blockers (Paré et al., 1998b). Two sets of passive properties were used: (1) a set with uniform leak conductance obtained from sharp-electrode recordings (Destexhe and Paré, 1999) and (2) a non-uniform leak model with low axial resistance, as obtained from dual-patch recordings (Stuart and Spruston, 1998).

Active properties. Active properties were simulated using Hodgkin and Huxley (Hodgkin and Huxley, 1952) type models for voltage-dependent Na^+, K^+, and Ca^{2+} conductances. The densities used were as follows (in mS/cm^2): 3–12 (soma and dendrites) for Na^+ and 5–10 (soma and dendrites) for K^+. Densities in the axon were chosen to be 5–10 times higher in the initial segment and nodes of Ranvier. Kinetics of the currents were taken from a model of hippocampal pyramidal cells (Traub and Miles, 1991), in which Na^+ inactivation was shifted by 10 mV toward hyperpolarized values to match voltage-clamp data of cortical pyramidal cells (Huguenard et al., 1988). Results were checked using different kinetic models for Na^+ and K^+ currents, as well as for different positions of the steady-state inactivation of Na^+ channels. In some simulations, Ca^{2+} and Ca^{2+}-dependent K^+ currents, as well as A-type K^+ currents, were used (for details, see Appendix).

Synaptic currents. Synaptic currents were simulated by two-state kinetic models for glutamate, AMPA, NMDA, and GABA type-A ($GABA_A$) receptor types (Destexhe et al., 1994). The densities of synapses were calculated in different regions of the cell based on morphological data (White, 1989; Larkman, 1991; DeFelipe and Farinas, 1992) and were (per 100 μm^2 of membrane) 10–20 ($GABA_A$, soma), 40–80 ($GABA_A$, axon initial segment), 8–12 ($GABA_A$, dendrites), and 55–65 (AMPA–NMDA, dendrites). This led to a total of 49,699 glutamatergic and 10,669 GABAergic synapses for the layer V cell shown in Figure 1*A* (16,563 and 3376, respectively, for the layer VI cell shown in Fig. 1*B*). Quantal conductances were assumed to be uniform (Williams and Stuart, 2002) and were estimated from fitting the model to recordings of miniature synaptic events (Destexhe and Paré, 1999). The quantal conductances obtained were of 1.2 and 0.6 nS for glutamatergic and GABAergic synapses, respectively.

Synaptic background activity. Synaptic background activity was simulated by random (Poisson-distributed) release events at all synapses. The release parameters were estimated by fitting the model to intracellular recordings *in vivo* before and after suppression of background activity (Paré et al., 1998b; Destexhe and Paré, 1999). Release rates in the range of 0.1–1 and 0.55–5.5 Hz at glutamatergic and GABAergic synapses, respectively, gave average membrane potentials, input resistances, and fluctuation levels consistent with intracellular recordings. A correlation was included between release events (cross-correlation peak of $c = 0.1$) (for details, see Destexhe and Paré, 1999). In these conditions, we calculated that the total membrane conductance attributable to inhibition is approximately four to five times larger than excitation, and, given the difference in driving force, excitatory and inhibitory currents are approximately balanced (with a slight excess for excitation).

Correlations. Correlations were introduced by forcing some of the synapses to corelease while keeping the random nature of the release at each synapse. This was achieved by generating N_0 Poisson-distributed random presynaptic trains and by redistributing these trains among the N synaptic sites in the model. If $N_0 < N$, all synapses still released randomly with identical statistical properties, but, at any given instant, some of the N synapses released simultaneously and were therefore "correlated." The N_0 inputs were redistributed randomly among the N synapses at every time step, such that the average correlation was the same for every pair of synapses, regardless of their location in the dendritic tree. Because correlations selectively affect the amplitude of voltage fluctuations (Destexhe and Paré, 1999), this procedure can be used to control voltage fluctuations (by changing N_0), with no change in the average conduc-

tance and membrane potential of the cell. Note that the correlation used corresponds to a pairwise Pearson correlation of ~0.1, which is consistent with the values measured experimentally for the "background" correlation in cerebral cortex (Zohary et al., 1994; Vaadia et al., 1995).

Static conductance. In some simulations, background activity was replaced by an equivalent static conductance. This conductance was obtained by inserting in each compartment a supplemental leak conductance, which was calculated to equate the average activity of the synapses converging to that compartment. The model obtained had a membrane potential, input resistance, and time constant that were equivalent to the model with background activity but had no membrane potential fluctuations.

Synaptic stimuli. Synaptic stimuli consisted of a supplementary set of AMPA-mediated synaptic conductances inserted at different locations in the dendritic tree. Stimulation intensity was adjusted by varying the number of synchronously activated AMPA synapses (quantal conductance of 1.2 nS), colocalized at the same dendritic sites. The stimulation was repeated every 50 msec. Successive stimuli can be considered as independent because the period was large compared with the typical duration of the responses (Fig. 2*B*). For each site, a total of 1200 stimulations (trials) were used to calculate the poststimulus time histogram (PSTH). For each parameter set, the model was run twice, with and without stimulus, and the spikes specifically evoked by the stimulus were obtained by subtracting spikes attributable to background activity. The time integral of the PSTH gives the probability that a somatic spike is specifically evoked by the stimulus, which is used as a measure of synaptic efficacy (for other measures, see London et al., 2002).

Results

We start by showing that background activity induces a stochastic dynamics that affects dendritic AP initiation and propagation. We next investigate the impact of individual synapses at the soma in this stochastic state, as well as how synaptic efficacy is modulated by different factors, such as morphology and the intensity of background activity itself. Finally, we investigate how this stochastic state affects the timing of synaptic events as a function of their position in the dendrites.

A stochastic state with facilitated action potential initiation

We first characterized how synaptic background activity affects the dynamics of AP initiation and propagation in dendrites. Dendritic AP propagation was simulated in computational models of morphologically reconstructed cortical pyramidal neurons, which included voltage-dependent currents in soma, dendrites, and axon (Fig. 1*A*, *top*) (see Materials and Methods). In quiescent conditions, backpropagating dendritic APs were reliable up to a few hundred micrometers from the soma (Fig. 1*A*, *bottom*, *Quiescent*), in agreement with dual soma–dendrite recordings *in vitro* (Stuart and Sakmann, 1994; Stuart et al., 1997b). In the presence of synaptic background activity, backpropagating APs were still robust but propagated over a more limited distance in the apical dendrite compared with quiescent states (Fig. 1*A*, *bottom*, *In vivo-like*), consistent with the limited backward invasion of apical dendrites observed with two-photon imaging of cortical neurons *in vivo* (Svoboda et al., 1997).

APs could also be initiated in dendrites after simulated synaptic stimuli. In quiescent conditions, the threshold for dendritic AP initiation was high (Fig. 1*B*, *left*, *Quiescent*), and the dendritic-initiated APs propagated forward only over limited distances (100–200 μm) (Fig. 1*C*, *Quiescent*), in agreement with previous observations (Stuart et al., 1997a; Golding and Spruston, 1998; Vetter et al., 2001). Interestingly, background activity tended to facilitate forward-propagating APs. Dendritic AP initiation was highly stochastic because of the presence of random fluctuations, but computing the probability of AP initiation revealed a signif-
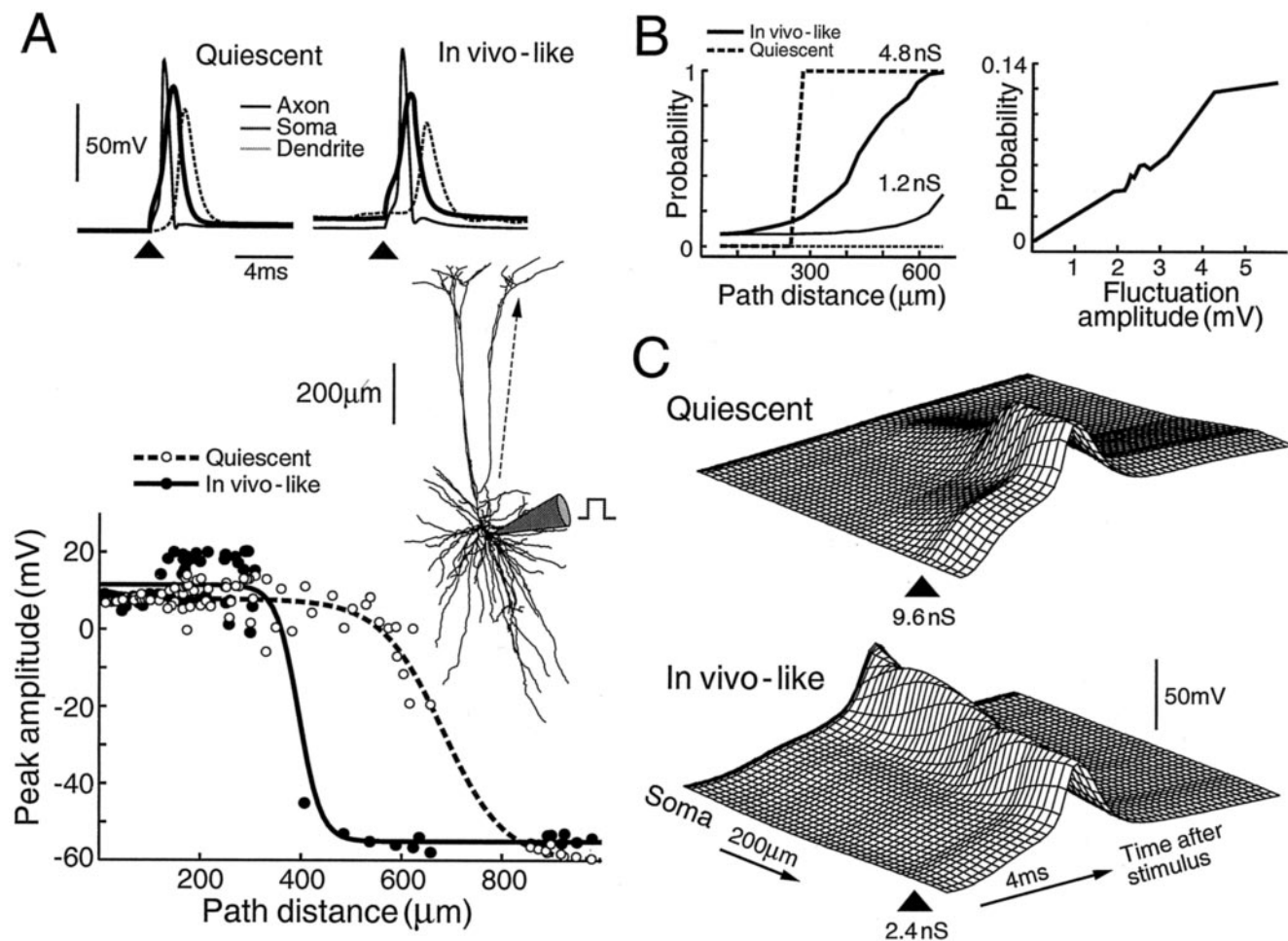
Figure 1. Dendritic action potential initiation and propagation under *in vivo*-like activity. *A*, Impact of background activity on AP backpropagation in a layer V cortical pyramidal neuron. *Top*, The respective timing of APs in soma, dendrite (300 μm from soma), and axon are shown after somatic current injection (*arrow*). *Bottom*, Backpropagation of the AP in the apical dendrite for quiescent (*open circles*) and *in vivo*-like (*filled circles*) conditions. The backward invasion was more restricted in the latter case. *B*, Impact of background activity on dendritic AP initiation. *Left*, Probability for initiating a dendritic AP shown as a function of path distance from soma for two different amplitudes of AMPA-mediated synaptic stimuli (*thick line*, 4.8 nS; *thin line*, 1.2 nS). *Right*, Probability of dendritic AP initiation (100 μm from soma) as a function of the amplitude of voltage fluctuations (1.2 nS stimulus). *C*, Impact of background activity on dendritic AP propagation. A forward-propagating dendritic AP was evoked in a distal dendrite by an AMPA-mediated EPSP (*arrow*). *Top*, In quiescent conditions, this AP only propagated within 100–200 μm, even for high-amplitude stimuli (9.6 nS shown here). *Bottom*, Under *in vivo*-like conditions, dendritic APs could propagate up to the soma, even for small stimulus amplitudes (2.4 nS shown here). *B* and *C* were obtained using the layer VI pyramidal cell described in Figure 2*B*.

icant effect of background activity (Fig. 1*B*, *left*, *In vivo-like*). The propagation of initiated APs was also stochastic, and a significant fraction (see below) of dendritic APs could propagate forward over large distances and reach the soma (Fig. 1*C*, *In vivo-like*), a situation that did not occur in quiescent states with low densities of Na^+ channels in dendrites.

To explain this effect of background activity on dendritic APs, we compared different background activities with equivalent conductance but different amplitudes of voltage fluctuations (see Materials and Methods). Figure 1*B* (*right*) shows that the probability of AP initiation, for fixed stimulation amplitude and path distance, was zero in the absence of fluctuations but steadily raised for increasing fluctuation amplitudes (all simulations were at equivalent voltage). This shows that subthreshold stimuli are occasionally boosted by depolarizing fluctuations. Propagating APs can also benefit from this boosting to help their propagation all the way up to the soma. In this case, the AP itself must be viewed as the stimulus that is boosted by the presence of depolarizing fluctuations. The same picture was observed for different morphologies, passive properties, and various densities and ki-

netics of voltage-dependent currents (see below): *in vivo*-like activity induced a stochastic dynamics in which backpropagating APs were minimally affected, but forward-propagating APs were facilitated. Thus, under *in vivo*-like conditions, subthreshold EPSPs can be occasionally boosted by depolarizing fluctuations and have a chance to initiate a dendritic AP, which itself has a chance to propagate and reach the soma.

Location independence of the impact of individual or multiple synapses

We next evaluated quantitatively the consequences of this stochastic dynamics of dendritic AP initiation in terms of the impact of individual EPSPs at the soma. In quiescent conditions, the model was adjusted to the passive parameters estimated from whole-cell recordings *in vitro* (Stuart and Spruston, 1998), yielding a relatively moderate passive voltage attenuation (Fig. 2*A*, *Quiescent*; 25–45% attenuation for distal events). Taking into account the high conductance and more depolarized conditions of *in vivo*-like activity showed a marked increase in voltage attenuation (Fig. 2*A*, *In vivo-like*; 80–90% attenuation). Computing the EPSP peak amplitude in
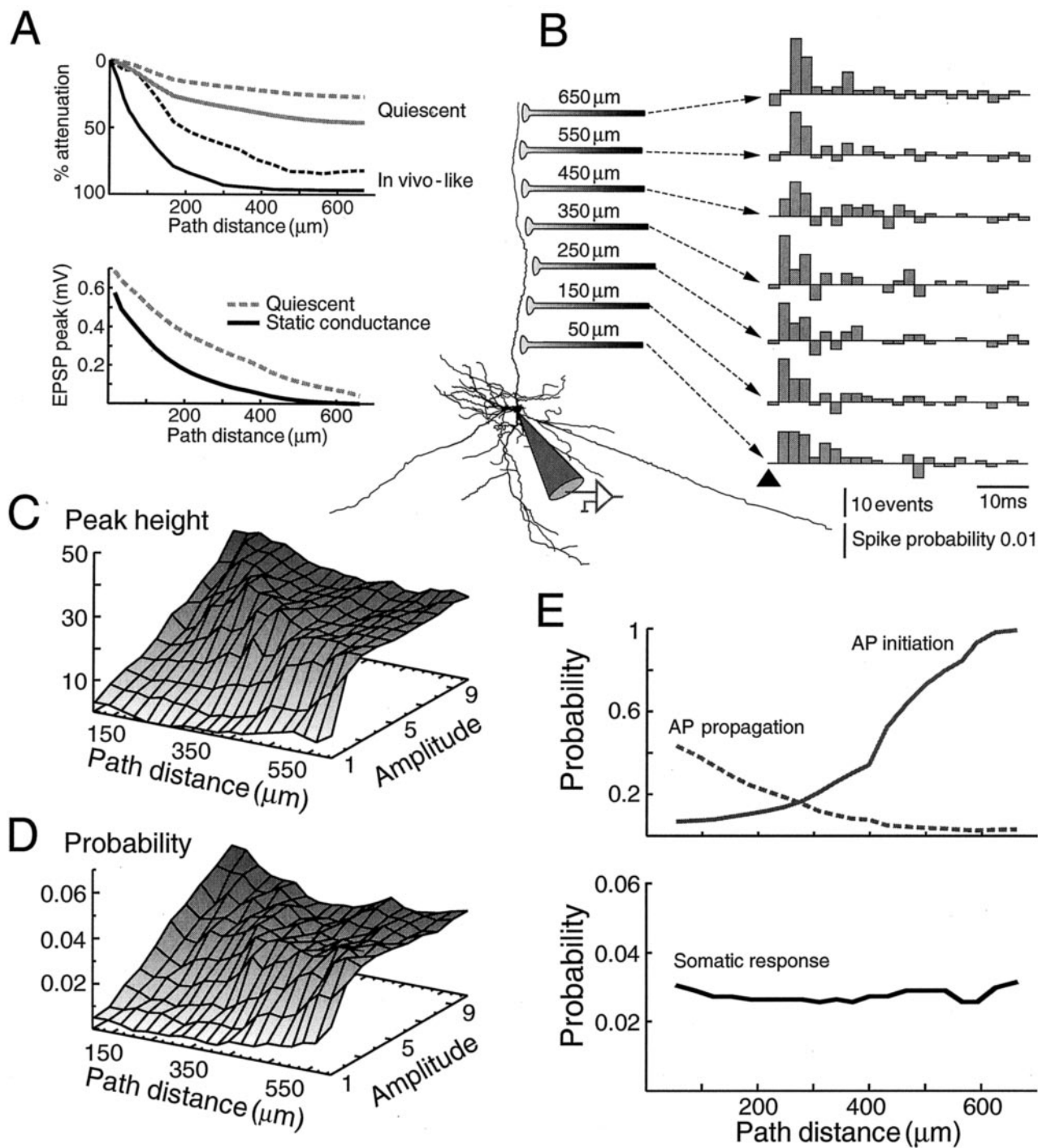
Figure 2. Independence of the somatic response to the location of synaptic stimulation under *in vivo*-like conditions. *A*, Impact of background activity on passive voltage attenuation. *Top*, Somatodendritic membrane potential profile at steady state after current injection at the soma (+0.4nA; layer VI cell shown in *B*). Two sets of passive properties were used: *solid lines*, from Destexhe and Paré (1999); *dashed lines*, from Stuart and Spruston (1998). *Bottom*, Peak EPSP at the soma as a function of path distance for AMPA-mediated 1.2 nS stimuli at different dendritic sites (dendritic branch shown in *B*). Peak EPSPs in quiescent conditions are compared with EPSPs obtained with a high static conductance. *B*, PSTHs of responses to identical AMPA-mediated synaptic stimuli (12 nS) at different dendritic locations (cumulated over 1200 trials after subtraction of spikes attributable to background activity). *C*, Peak of the PSTH as a function of stimulus amplitude (from 1 to 10 coactivated AMPA synapses; conductance range, 1.2–12 nS) and distance to soma. *D*, Integrated PSTH (probability that a somatic spike was specifically evoked by the stimulus) as a function of stimulus amplitude and distance to soma. Both *C* and *D* show reduced location dependence. *E*, *Top*, Comparison of the probability of evoking a dendritic spike (*AP initiation*) and the probability that an evoked spike translated into a somatic–axonal spike (*AP propagation*). Both were represented as a function of the location of the stimulus (AMPA-mediated stimulus amplitudes of 4.8 nS). *Bottom*, Probability of somatic spike specifically evoked by the stimulus, which was obtained by multiplying the two curves above. This probability was nearly location independent.

these conditions revealed an attenuation with distance (Fig. 2*A*, *lower panel*), which was more pronounced if background activity was represented by an equivalent static (leak) conductance (see Materials and Methods). Thus, the high-conductance component of the

background activity enhances the location-dependent impact of EPSPs and leads to a stronger individualization of the different dendritic branches (London and Segev, 2001; Rhodes and Llinás, 2001).

A radically different conclusion was reached if voltage fluctu-

ations were taken into account. In this case, responses were highly irregular, and the impact of individual synapses was assessed by computing the PSTH over long periods of time with repeated stimulation of single or groups of colocalized excitatory synapses (see Materials and Methods). The PSTHs obtained for stimuli occurring at different distances from the soma (Fig. 2*B*) show that the "efficacy" of these synapses is approximately location independent, as calculated from either the peak (Fig. 2*C*) or the integral of the PSTH (Fig. 2*D*). The latter can be interpreted as the probability that a somatic spike is specifically evoked by a synaptic stimulus. Using this measure of synaptic efficacy, we conclude that, under *in vivo*-like conditions, the impact of individual synapses on the soma is nearly independent on their dendritic location, despite a severe voltage attenuation.

Mechanisms underlying location independence

To show that this location-independent mode depends on forward-propagating dendritic APs, we selected, for a given synaptic location, all trials that evoked a somatic spike. These trials represented a small portion of all trials: from 0.4 to 4.5% depending on the location and the strength of the synaptic stimuli. For these "successful" selected trials, the somatic spike was always preceded by a dendritic spike evoked locally by the stimulus. In the remaining "unsuccessful" trials, there was a proportion of stimuli (55–97%) that evoked a dendritic spike but failed to evoke somatic spiking. This picture was the same for different stimulation sites: a fraction of stimuli evokes dendritic spikes, and a small fraction of these dendritic spikes successfully evokes a spike at the soma–axon.

We analyzed the latter aspect by representing the probabilities of initiation and propagation along the distance axis (Fig. 2*E*). There was an asymmetry between these two measures: the chance of evoking a dendritic AP was lower for proximal stimuli and increased with distance (Fig. 2*E*, *AP initiation*), because the local input resistance varies inversely with dendrite diameter and is higher for thin (distal) dendritic segments. On the other hand, the chance that a dendritic AP propagates down to the soma and leads to soma–axon APs was higher for proximal sites and gradually decreased with distance (Fig. 2*E*, *AP propagation*). Remarkably, these two effects compensated such that the probability of evoking a soma–axon AP (the product of these two probabilities) was approximately independent on the distance to soma (Fig. 2*E*, *Somatic response*). This effect was observed only in the presence of conductance-based background activity and was not present in quiescent conditions or by using current-based models of synapses (data not shown). These results show that the location-independent impact of synaptic events under *in vivo*-like conditions is attributable to a compensation between an opposite distance dependence of the probabilities of AP initiation and propagation.

The same dynamics were present in four different pyramidal cell morphologies (Fig. 3), suggesting that this principle may apply to a large variety of dendritic morphologies. It was also robust to variations in ion channel densities and kinetics, such as NMDA conductances (Fig. 4*A*), passive properties (Fig. 4*B*), and different types of ion channels (Fig. 4*C*), including high distal densities of leak and hyperpolarization-activated I_h conductances (Fig. 4*C*, *gray line*). In the latter case, the presence of I_h affected EPSPs in the perisomatic region, in which there is a significant contribution of passive signaling, but synaptic efficacy was remarkably location independent for the remaining part of the dendrites in which the I_h density was highest (see Appendix). Location independence was also robust to changes in membrane excitability
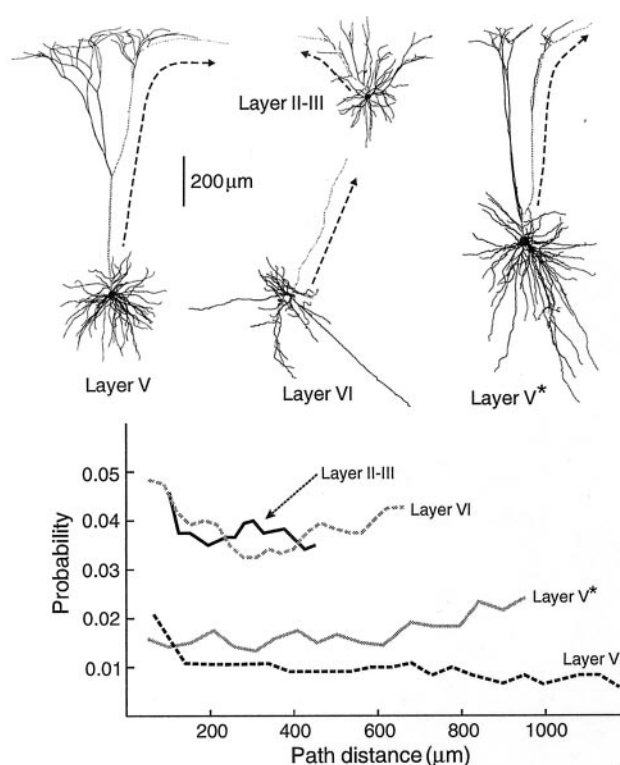

Figure 3. Location-independent impact of synaptic inputs for different cellular morphologies. The somatic response to AMPA stimulation (12 nS amplitude) is indicated for different dendritic sites (corresponding branches are indicated by *dashed arrows*; equivalent electrophysiological parameters and procedures as in Fig. 2*B–D*) for four different cells (1 layer II–III, 2 layer V, and 1 layer VI) based on cellular reconstructions from cat cortex (Douglas et al., 1991; Contreras et al., 1997). Somatic responses (integrated PSTH) are represented against the path distance of the stimulation sites. In all cases, the integrated PSTH shows location independence, but the averaged synaptic efficacy was different for each cell type.

(Fig. 4*D,E*) and shifts in the Na$^+$ current inactivation (Fig. 4*F*). Most of these variations changed the absolute probability of evoking spikes but did not affect the location independence induced by background activity. The location-independent synaptic efficacy was lost when the dendrites had too strong K$^+$ conductances, with either high I_{KA} in distal dendrites (Fig. 4*C*, *black dotted line*) or a high ratio between K$^+$ and Na$^+$ conductances (Fig. 4*E*). In other cases, synaptic efficacy was larger for distal dendrites (Fig. 4*D*, high excitability, *F*, inactivation shift of 0).

Activity-dependent modulation of synaptic efficacy

To determine how the efficacy of individual synapses varies as a function of the intensity of synaptic background activity, we repeated the same stimulation paradigms as in Figure 2 but by varying individually the release rates of excitatory (Fig. 5*A*) or inhibitory (Fig. 5*B*) inputs of the background, by varying both (Fig. 5*C*), or by varying the correlation with fixed release rates (Fig. 5*D*). In all cases, synaptic efficacy (integrated PSTH for stimuli that were subthreshold under quiescent conditions) depended on the particular properties of background activity but remained location independent. In the case of "balanced" excitatory and inhibitory inputs (Fig. 5*C*), background activity could be changed continuously from quiescent to *in vivo*-like conditions. In this case, the probability steadily rose from zero (Fig. 5*C*, *clear region*), showing that subthreshold stimuli can evoke detectable responses in the presence of background activity, and reached a "plateau" at which synaptic efficacy was independent of both
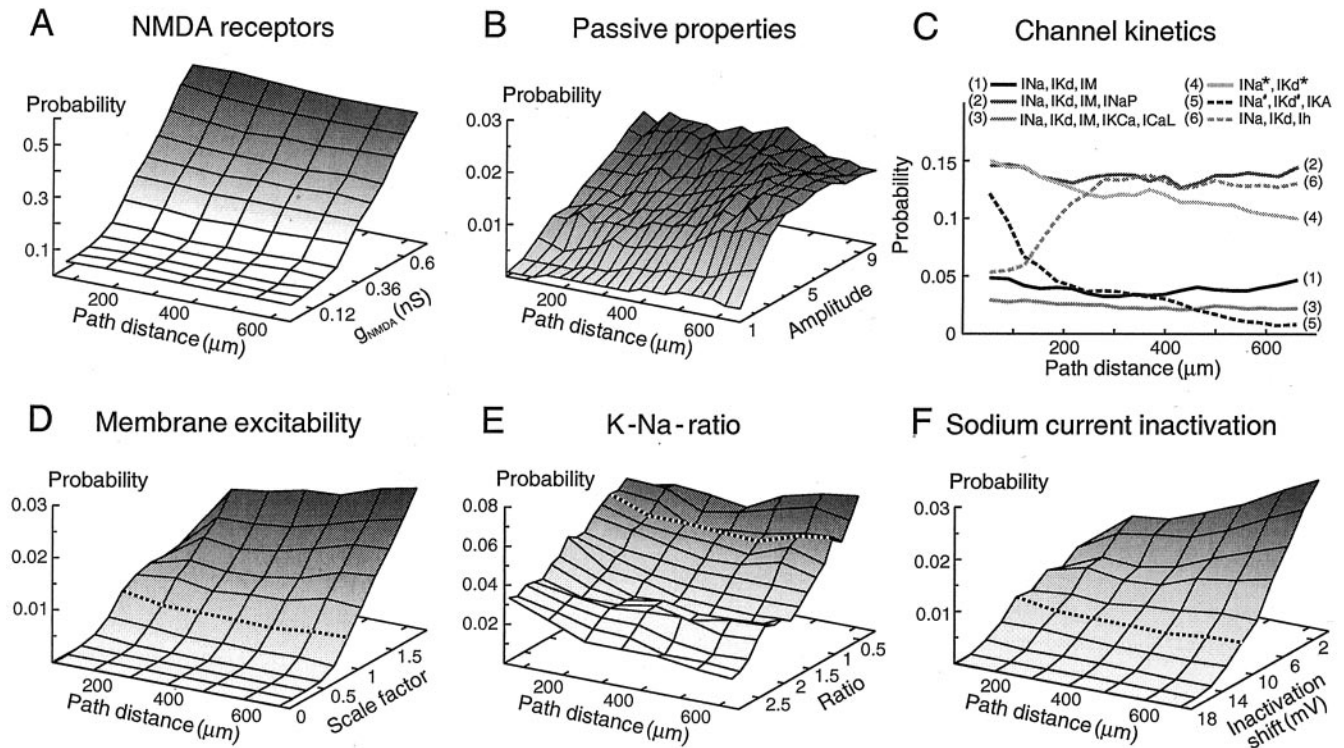
Figure 4. Location independence for various passive and active properties. *A,* Synaptic efficacy as a function of path distance and conductance of NMDA receptors. The quantal conductance (g_{NMDA}) was varied between 0 and 0.7 nS, which corresponds to a fraction of 0 to ~60% of the conductance of AMPA channels (Zhang and Trussell, 1994; Spruston et al., 1995). NMDA receptors were colocalized with AMPA receptors (release frequency of 1 Hz), and stimulation amplitude was 12 nS. *B,* Synaptic efficacy as a function of path distance and stimulation amplitude for a non-uniform passive model (Stuart and Spruston, 1998) (see Appendix). *C,* Synaptic efficacy as a function of path distance for different ion channel models or different kinetic models of the same ion channels (stimulation, 12 nS) (for details of the models, see Appendix). *D,* Synaptic efficacy as a function of path distance and membrane excitability. Both Na^+ and K^+ conductance densities were changed by a common multiplicative scaling factor. The *dotted line* indicates a dendritic conductance density of 8.4 mS/cm ^{2} for the Na^+ current and 7 mS/cm ^{2} for the delayed rectifier K^+ current. The stimulation amplitude was, in all cases, 12 nS. *E,* Synaptic efficacy obtained by changing the ratio between Na^+ and K^+ conductances responsible for action potentials (conductance density of 8.4 mS/cm ^{2} for I_{Na} ; the *dotted line* indicates 7 mS/cm ^{2} for I_{Kd}). *F,* Synaptic efficacy as a function of path distance obtained by varying the steady-state inactivation of the fast Na^+ current. The inactivation curve was shifted with respect to the original model (Traub and Miles, 1991) toward hyperpolarized values (stimulation amplitude, 12 nS). The *dotted line* indicates a 10 mV shift, which approximately matches the voltage-clamp data of cortical pyramidal cells (Huguenard et al., 1988). All simulations were done using the layer VI cell in which AMPA-mediated synaptic stimuli were applied at different sites along the dendritic branch indicated by a *dashed arrow* in Figure 3.

synapse location and background intensity (Fig. 5C, *dark region*). This region corresponds to estimates of background activity on the basis of intracellular recordings *in vivo* (Destexhe and Paré, 1999). Thus, it seems that synaptic inputs are location independent for a wide range of background activities and intensities. Modulating the correlation, or the respective weight of excitation and inhibition, allows the network to globally modulate the efficacy of all synaptic sites at once.

Location dependence of the timing of synaptic events
We next tested whether location independence also applies to the timing of synaptic events. Figure 6A illustrates the somatic membrane potential after synaptic stimuli at different locations. In quiescent conditions, as predicted by cable theory (Segev et al., 1995; Koch, 1999), proximal synaptic events led to fast rising and fast decaying somatic EPSPs, whereas distal events were attenuated in amplitude and slowed in duration (Fig. 6A, *Quiescent*). The time-to-peak of EPSPs increased monotonically with distance (Fig. 6B, *Quiescent*). In the presence of background activity, the average amplitude of these voltage deflections was much less dependent on location (Fig. 6A, *In vivo-like*), consistent with the PSTHs in Figure 2B, and the time-to-peak of these events was only weakly dependent on the location of the synapses in dendrites (Fig. 6B, *In vivo-like*). Thus, *in vivo*-like conditions seem to set the dendrites into a fast-conducting mode, in which the tim-

ing of synaptic inputs shows little dependence on their distance to soma.

To investigate the basis of this fast-conducting mode, we simulated the same paradigm by varying a number of parameters. First, to check whether this effect could be attributable to the decreased membrane time constant as a result of the high conductance imposed by synaptic background activity, we replaced background activity by an equivalent static conductance, which led to an intermediate location-dependent relationship (Fig. 6C, *Quiescent, static conductance*) between the quiescent and *in vivo*-like cases depicted above. The reduced time constant therefore can account for some, but not all, of the diminished location dependence of the timing. Second, to check for contributions of dendritic Na^+ channels, we ran the same stimulation protocol under *in vivo*-like conditions but by selectively removing Na^+ channels from dendrites. This also led to an intermediate location dependence (Fig. 6C, *In vivo-like,* $g_{Na} = 0$), suggesting that Na^+-dependent mechanisms underlie the further reduction of timing beyond the high-conductance effect. Finally, to show that this further reduction is attributable to dendritic APs, we used a quiescent state with equivalent static conductance but higher dendritic excitability (Na^+ and K^+ conductances that were twice as large), such that strong synaptic stimuli can evoke reliable forward-propagating dendritic APs. In this case only, the reduced location dependence of the timing could be fully reconstructed

(Fig. 6*C*, *Quiescent, static conductance, high dendritic g_{Na}*). The dependence on dendritic APs was also confirmed by the intermediate location dependence obtained when EPSPs were constructed from trials that did not contain dendritic APs (Fig. 6*B*, *No dendritic spikes*). This analysis shows that the fast-conducting mode is attributable to forward-propagating APs in dendrites of fast time constant.

Discussion

In this paper, we modeled high-conductance states in neocortical pyramidal neurons that are associated with a depolarized and highly fluctuating membrane potential, as shown by intracellular measurements *in vivo*, in anesthetized (Contreras et al., 1996; Paré et al., 1998b) or awake animals (Matsumura et al., 1988; Steriade et al., 2001). The simulations suggest that these high-conductance states set pyramidal neurons into a stochastic integrative mode that is fast-conducting and in which the impact of inputs is location independent. The underlying mechanism depends on forward-propagating APs. The high conductance of background activity lowers the membrane time constant and enhances passive voltage attenuation; this enhanced attenuation limits the passive spread to soma and the triggering of backpropagating APs by dendritic stimuli and therefore leaves the opportunity for stimuli to influence the soma by forward-propagating APs. At the same time, the voltage fluctuations associated with synaptic activity induce a stochastic dynamics that facilitates the initiation and propagation of dendritic APs (this effect is consistent with the facilitation of dendritic APs by EPSPs shown by Stuart and Häusser, 2001). The combined result of these actions is that colocalized synaptic events have a small (but non-zero) chance to trigger a dendritic spike, which itself has a chance to propagate rapidly to the soma in which it can participate in firing the soma–axon. In contrast with an axon, however, the dynamics is here stochastic in nature, and there is a complex dependence on distance for the probability of AP initiation and propagation (Fig. 2*E*). These effects compensate such that the impact of a given synapse is approximately independent of its position in the dendrite. Different regions of the neuron, including distal dendrites, can therefore efficiently vote for firing the cell. The same dynamics was observed for different morphologies (Fig. 3), different passive and active properties (Fig. 4), and various background activities (Fig. 5).

This stochastic integrative mode was present despite considerable variations in the type or kinetics of ions channels in dendrites. It was present with voltage-dependent Ca^{2+} channels or with high distal densities of the hyperpolarization-activated current I_h (Fig. 4*C*), similar to the densities measured in the apical dendrite of layer V neocortical pyramidal neurons (Stuart and Spruston, 1998; Larkum et al., 1999a,b; Williams and Stuart, 2000a; Berger et al., 2001) (for a model, see Rhodes and Llinás, 2001). Our study is therefore applicable to a wide range of dendritic excitabilities typical of cortical neurons. Because the mechanism is dependent on forward dendritic spikes, it can fail in situation with suppressed dendritic spike activity, such as strong
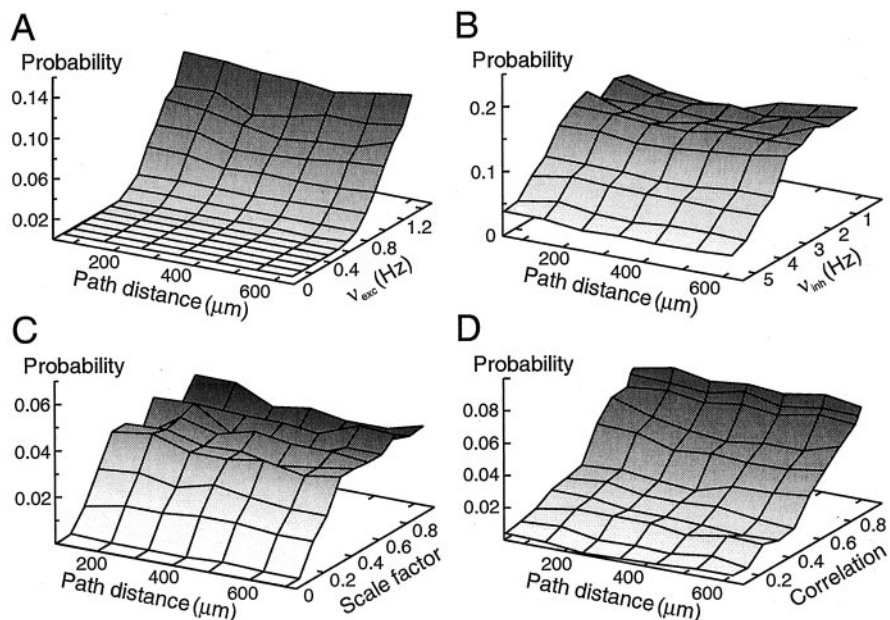

Figure 5. Modulation of synaptic efficacy by background activity. *A*, Integrated PSTH obtained for different intensities of background activity obtained by varying the release rates at glutamatergic synapses (ν_{exc}) while keeping the release rates fixed at GABAergic synapses ($\nu_{inh} = 5.5$ Hz). *B*, Integrated PSTH obtained by varying the release rates at inhibitory synapses (ν_{inh}) with fixed excitatory release rates ($\nu_{exc} = 1$ Hz). *C*, Integrated PSTH obtained by varying both excitatory and inhibitory release rates, using the same scaling factor. The plateau region (*dark*) shows that the global efficacy of synapses and their location independence are robust to changes in the intensity of network activity. *D*, Integrated PSTH obtained for fixed release rates but different background correlations. In all cases, the integrated PSTHs represent the probability that a spike was specifically evoked by synaptic stimuli (12 nS, AMPA-mediated), as in Figure 2 *D*.

dendritic K$^+$ conductances (Fig. 4*C*, I_{Na}^*, I_{Kd}^*, I_{KA}; *E*, large K/Na ratio). This suggests that this mechanism would be particularly relevant to states in which K$^+$ conductances are downregulated. This is the case for aroused states, which are maintained by neuromodulators such as acetylcholine, noradrenaline, or serotonin, all of which downregulate K$^+$ conductances in neocortical neurons (McCormick, 1992).

The fact that the same dynamics can be reproduced in different morphologies (Fig. 3) suggests that the location-independent efficacy of synapses could apply to different types of neurons, regardless of the complexity of their dendritic arborization. If this principle is true, cortical neurons would be free to optimize their dendritic arbor based on connectivity constraints only (and not on synaptic weight for example). This is valid, however, only for colocalized synaptic events, as investigated here. There is a large spectrum of possibilities that should be analyzed, including the synchrony of multiple inputs, their kinetics and receptor type, and the joint impact of paired synaptic events as a function of their relative distance and timing. Such an analysis may reveal a dependence on the local structure of the dendrites, similar to the "dendritic subunits" postulated in previous models of dendritic integration (Mel, 1994).

Another interesting property of this stochastic integrative mode is that synaptic efficacy is modulable by network activity. Changing the balance of excitation–inhibition, release rates, or correlation in background activity can reconfigure synaptic efficacies, but it does so by preserving location independence (Fig. 5). The model predicts that the highest synaptic efficacies should be obtained for states of intense "spontaneous" network activity, a somewhat counter-intuitive result. Note that the stochastic aspect also implies that neocortical neurons would have to use population codes to reliably encode information. In this respect,
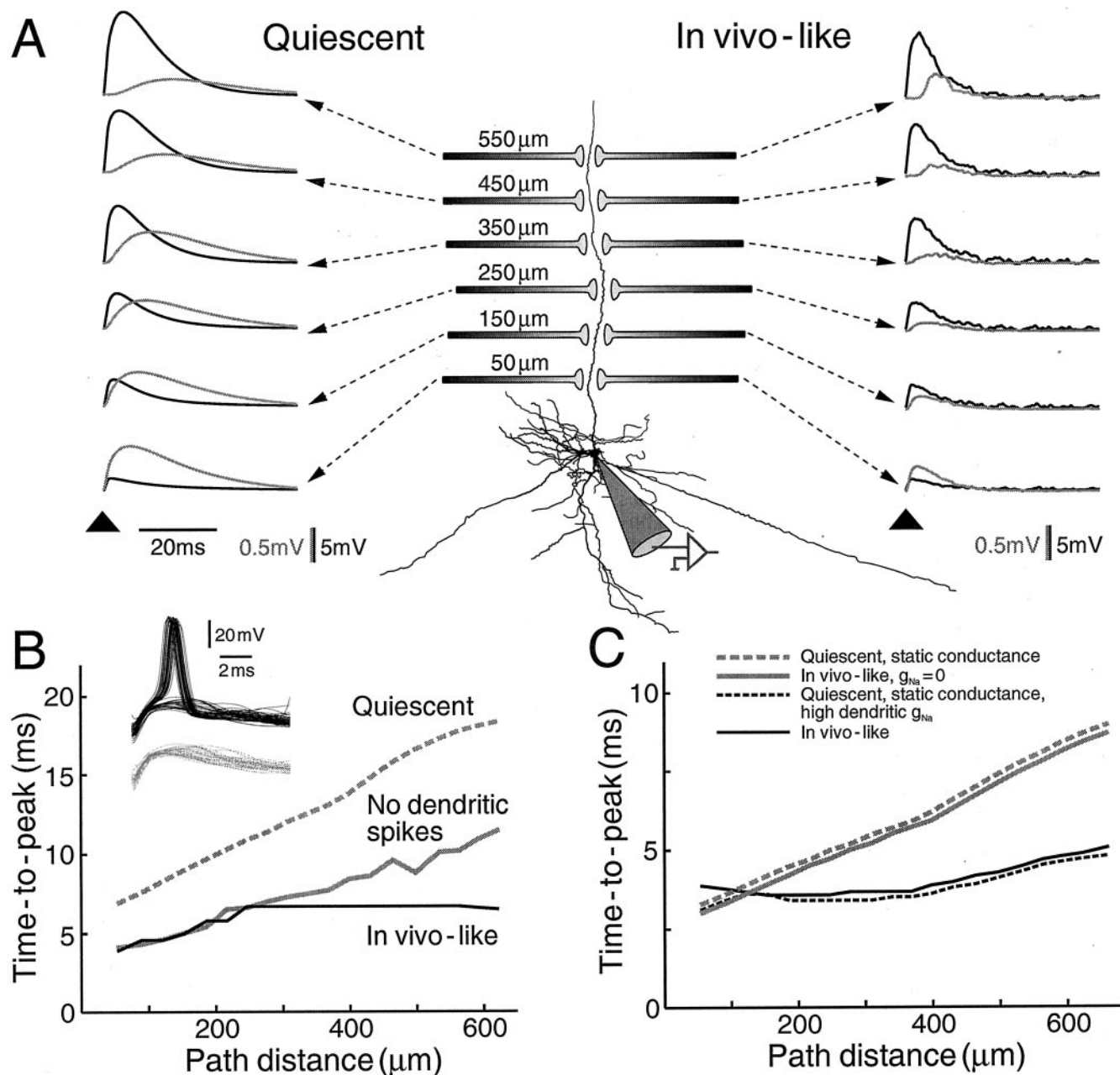
Figure 6. Fast conduction of dendrites under in vivo-like conditions. A, Somatic (black) and dendritic (gray) voltage deflections after stimuli at different locations (somatic responses are shown with a magnification of 10×). There was a reduction of the location dependence at the soma under in vivo-like conditions (averages over 1200 traces) compared with the quiescent state (all stimuli were 1.2 nS, AMPA-mediated). B, Location dependence of the timing of EPSPs. In the quiescent state, the time-to-peak of EPSPs increased approximately linearly with the distance to soma (Quiescent). This dependence on location was markedly reduced under in vivo-like conditions (In vivo-like), defining a fast-conducting state of the dendrites. This location dependence was affected by removing dendritic APs (No dendritic spikes). Inset, Examples of dendritic EPSPs at the site of the synaptic stimulation (50 traces, stimulation with 8.4 nS at 300 μm from soma) are shown under in vivo-like conditions (black) and after dendritic APs were removed (gray). C, Mechanism underlying fast dendritic conduction. Replacing background activity by an equivalent static conductance (Quiescent, static conductance) or suppressing dendritic Na$^+$ channels (In vivo-like, $g_{Na} = 0$) led to an intermediate location dependence of EPSP time-to-peak. On the other hand, using high dendritic excitability together with strong synaptic stimuli (12 nS) evoked reliable dendritic APs and yielded a reduced location dependence of the time-to-peak in quiescent conditions (Quiescent, static conductance, high dendritic g_{Na}), comparable with in vivo-like conditions. The fast-conducting mode is therefore attributable to forward-propagating dendritic APs in dendrites of fast time constant.

the modulation of synaptic efficacies by network activity suggests that the number of neurons that respond to a given stimulus is determined by the spontaneous activity of the network.

Location independence was found and modeled in a number of previous studies (De Schutter and Bower, 1994; Magee and Cook, 2000; Andrásfalvy and Magee, 2001; London and Segev, 2001; Rudolph et al., 2001). In hippocampal pyramidal neurons, synaptic conductances are scaled according to their distance to

soma to compensate for dendritic filtering (Magee and Cook, 2000; Andrásfalvy and Magee, 2001) (but see London and Segev, 2001), a situation that does not seem to apply to neocortical neurons (Williams and Stuart, 2002). In Purkinje cells, background activity can induce location independence for synchronized synaptic inputs by a subthreshold, Ca^{2+}-mediated mechanism (De Schutter and Bower, 1994). In contrast, we show here a stochastic mechanism based on Na$^+$-dependent APs that equally

applies to single or synchronized synaptic inputs. It would be interesting to investigate the same behavior in other cell types, such as thalamic neurons, which also contain Na^+ and Ca^{2+} channels in their dendrites (Destexhe et al., 1998; Williams and Stuart, 2000b) and are subject to intense synaptic background activity *in vivo* (Contreras et al., 1996).

Some of the present observations suggest additional theoretical work. First, the fact that dendrites subject to high-conductance fluctuations can compensate for the opposite location-dependent effects of AP initiation and propagation (Fig. 2*E*) should be investigated using the stochastic cable theory to understand the underlying mechanisms. Second, the observation of an increased traffic of Na^+-dependent dendritic APs in these conditions suggests possible consequences on spike-timing dependent plasticity (STDP). STDP is thought to occur according to the relative timing between release events and postsynaptic APs (for review, see Bi and Poo, 2001). The present results suggest that, during active states, a significant fraction of postsynaptic APs are local dendritic spikes, which opens the possibility for local dendritic regions to manage their synaptic plasticity mechanisms independently of the soma (Golding et al., 2002). Additional work is needed to evaluate to what extent such a local plasticity rule could duplicate the computational power of cortical neurons (Mel, 1994).

Finally, this model formulates a series of experimentally testable predictions. The predicted stochastic initiation and propagation of dendritic APs should be observable by single-cell imaging techniques *in vivo* (Svoboda et al., 1997), if such recordings can be made in activated states with desynchronized EEG. The prediction that location-dependent synaptic efficacies should become location independent in the presence of intense background activity could be tested by using dual soma–dendrite recordings (for methods, see Stuart and Sakmann, 1994; Larkum et al., 1999a; Berger et al., 2001; Williams and Stuart, 2002). This could be performed in slices either with artificially induced active states (Buhl et al., 1998; Brumberg et al., 2000) or by recreating *in vivo*-like activity by intracellular injection of fluctuating conductances (Destexhe et al., 2001). In both cases, protocols similar to Figure 2*B*–*D* could be used to calculate the efficacy of synaptic conductance waveforms injected in dendrites and to compare the efficacy between quiescent and active states.

Appendix
This appendix contains details of the different models used in the paper. Computational models and scripts for the NEURON simulation environment are available at http://cns.iaf.cnrs-gif.fr/supplement.html.

Morphology
Simulations were performed using multicompartment models of morphologically reconstructed neocortical pyramidal neurons from layer II–III, V, and VI of cat parietal cortex (Contreras et al., 1997), as well as a layer V cell from cat cortex (Douglas et al., 1991) (Fig. 3) with both simple and detailed axonal geometry (Mainen et al., 1995; Paré et al., 1998a). In all models, passive properties and active conductances in dendrites were changed to account for the surface correction attributable to dendritic spines, assuming that ~45% of the dendritic membrane area are represented by spines (DeFelipe and Farinas, 1992).

Uniform passive model
Passive model parameters were adjusted to intracellular (sharp-electrode) recordings obtained after application of TTX and synaptic blockers (Destexhe and Paré, 1999), yielding an axial resis-

tance $R_a = 250 \ \Omega$ cm, a membrane resistance $R_m = 22$ kΩ cm^2 in soma and dendrites ($R_m = 50 \ \Omega$ cm^2 in axon), and membrane capacity $C_m = 1 \ \mu$F/cm^2 in soma and dendrites ($C_m = 0.04 \ \mu$F/cm^2 in initial and myelinated segments of axon).

Nonuniform passive model
A non-uniform leak model obtained from dual-patch recordings in neocortical layer V pyramidal neurons (Stuart and Spruston, 1998) was used with $C_m = 1.54 \ \mu$F/cm^2 in soma and dendrites ($C_m = 0.04 \ \mu$F/cm^2 in initial and myelinated segments of axon), and $R_a = 68 \ \Omega$ cm and $R_m = 50 \ \Omega$ cm^2 in axonal nodes of Ranvier. The membrane resistance in dendrites scaled in a sigmoidal manner with path distance, with values $R_m(\text{end}) = 5.36$ kΩ cm^2, $R_m(\text{soma}) = 39.06$ kΩ cm^2, steep = 50 μm, and $d_{\text{half}} = 300 \ \mu$m.

Active membrane conductances
Voltage-dependent conductances were inserted in the soma, dendrites, and the axon. Currents included the fast sodium current I_{Na}, the delayed rectifier potassium current I_{Kd}, a slow voltage-dependent potassium current I_M, a Ca^{2+}-dependent potassium current (C-current) $I_{K[Ca]}$, a high-threshold Ca^{2+} current (L-current) I_{CaL}, a persistent sodium current I_{NaP}, an A-type potassium current I_{KA}, and a hyperpolarization-activated conductance I_h. All currents were described by Hodgkin–Huxley-type models (Hodgkin and Huxley, 1952). Various combinations and densities in dendrites and soma were used, as follows.

I_{Na}, I_{Kd}, I_M
The standard kinetic models for these currents were taken from a model of hippocampal pyramidal cells (see Materials and Methods) (Traub and Miles, 1991), adjusted to match voltage-clamp data of cortical pyramidal cells (Huguenard et al., 1988). In the standard setup, constant peak conductance densities of 8.4 mS/cm^2 (soma and dendrites; 84 mS/cm^2 in axonal initial segment and nodes of Ranvier) for I_{Na}, 7 mS/cm^2 (soma and dendrites; 70 mS/cm^2 in axonal initial segment and nodes of Ranvier) for I_{Kd}, and 0.35 mS/cm^2 (soma and dendrites) for I_M (no I_M in axon) were used. These densities correspond to the values found experimentally in adult hippocampal pyramidal neurons (Magee and Johnston, 1995).

I_{Na}, I_{Kd}, I_M, $I_{K[Ca]}$, I_{CaL}
These currents are as the standard model with additional Ca^{2+}-dependent potassium current (for kinetics, see Yamada et al., 1989) with conductance density of 1 mS/cm^2 in dendrites and soma and high-threshold Ca^{2+} current I_{CaL} (for kinetics, see McCormick and Huguenard, 1992) with peak conductance density of 3 and 1.5 mS/cm^2 for proximal and distal dendrites, respectively.

I_{Na}, I_{Kd}, I_M, I_{NaP}
These currents are as the standard model with an additional persistent sodium current I_{NaP} (for kinetics, see French et al., 1990; McCormick and Huguenard, 1992) with conductance density of 0.1 mS/cm^2 in soma and dendrites.

$I_{Na}{}^*$, $I_{Kd}{}^*$
These currents are described by a different model of action potential generation, in which the fast Na^+ current and the delayed rectifier K^+ current were taken from a previous model of cortical pyramidal neurons (Mainen et al., 1995). Peak conductance densities were 8.4 mS/cm^2 (soma and dendrites; 84 mS/cm^2 in axon initial segment) for $I_{Na}{}^*$ and 7.0 mS/cm^2 (soma and dendrites; 70 mS/cm^2 in axon initial segment) for $I_{Kd}{}^*$.

$I_{Na}{}^{*}$, $I_{Kd}{}^{*}$, I_{KA}

These currents are according to a model of action potential generation for hippocampal pyramidal neurons (Migliore et al., 1999), including an A-type K^{+} current, which conductance density linearly increased with path distance (for details, see Migliore et al., 1999). Conductance densities were as follows: 7.4 mS/cm^{2} (soma and dendrites; 1860 mS/cm^{2} in axon initial segment and nodes of Ranvier) for $I_{Na}{}^{*}$, 10 mS/cm^{2} (soma and dendrites; 2500 mS/cm^{2} in axon initial segment and nodes of Ranvier) for $I_{Kd}{}^{*}$, and 48 mS/cm^{2} for I_{KA} in the soma. Two different kinetics for proximal and distal I_{KA} were used, with densities increasing with 48 mS/cm^{2} per 100 μm.

I_{Na}, $I_{Kd,}$ I_{h}

These currents are as the standard model for I_{Na} and I_{Kd} with an additional hyperpolarization-activated conductance I_{h} (kinetics and density according to non-uniform model by Stuart and Spruston, 1998): sigmoidal scaling with path distance, peak conductance density of 0.02 mS/cm^{2} at soma and 20 mS/cm^{2} in most distal dendrites, $d_{half} = 400$ μm, and steep $= 50$ μm.

References

Andrásfalvy BK, Magee JC (2001) Distance-dependent increase in AMPA receptor number in the dendrites of adult hippocampal CA1 pyramidal neurons. J Neurosci 21:9151–9159.

Andreasen M, Lambert JD (1995) Regenerative properties of pyramidal cell dendrites in area CA1 of the rat hippocampus. J Physiol (Lond) 483:421–441.

Barrett JN (1975) Motoneuron dendrites: role in synaptic integration. Fed Proc 34:1398–1407.

Benardo LS, Masukawa LM, Prince DA (1982) Electrophysiology of isolated hippocampal pyramidal dendrites. J Neurosci 2:1614–1622.

Berger T, Larkum ME, Lüscher HR (2001) High I(h) channel density in the distal apical dendrite of layer V pyramidal cells increases bidirectional attenuation of EPSPs. J Neurophysiol 85:855–868.

Bernander O, Douglas RJ, Martin KA, Koch C (1991) Synaptic background activity influences spatiotemporal integration in single pyramidal cells. Proc Natl Acad Sci USA 88:11569–11573.

Bi G, Poo M (2001) Synaptic modification by correlated activity: Hebb's postulate revisited. Annu Rev Neurosci 24:139–166.

Borg-Graham LJ, Monier C, Frégnac Y (1998) Visual input evokes transient and strong shunting inhibition in visual cortical neurons. Nature 393:369–373.

Brumberg JC, Sanchez-Vives MV, McCormick DA (2000) Waking the sleeping slice. Soc Neurosci Abstr 26:736.7.

Buhl EH, Tamas G, Fisahn A (1998) Cholinergic activation and tonic excitation induce persistent gamma oscillations in mouse somatosensory cortex in vitro. J Physiol (Lond) 513:117–126.

Cash S, Yuste R (1999) Linear summation of excitatory inputs by CA1 pyramidal neurons. Neuron 22:383–394.

Contreras D, Timofeev I, Steriade M (1996) Mechanisms of long-lasting hyperpolarizations underlying slow sleep oscillations in cat corticothalamic networks. J Physiol (Lond) 494:251–264.

Contreras D, Destexhe A, Steriade M (1997) Intracellular and computational characterization of the intracortical inhibitory control of synchronized thalamic inputs in vivo. J Neurophysiol 77:335–350.

Crill WE, Schwindt PC (1995) Amplification of synaptic current by persistent sodium conductance in apical dendrite of neocortical neurons. J Neurophysiol 74:2220–2224.

DeFelipe J, Farinas I (1992) The pyramidal neuron of the cerebral cortex: morphological and chemical characteristics of the synaptic inputs. Prog Neurobiol 39:563–607.

De Schutter E, Bower JM (1994) Simulated responses of cerebellar Purkinje cells are independent of the dendritic location of granule cell synaptic inputs. Proc Natl Acad Sci USA 91:4736–4740.

Destexhe A, Paré D (1999) Impact of network activity on the integrative properties of neocortical pyramidal neurons in vivo. J Neurophysiol 81:1531–1547.

Destexhe A, Mainen ZF, Sejnowski TJ (1994) An efficient method for computing synaptic conductances based on a kinetic model of receptor binding. Neural Comput 6:14–18.

Destexhe A, Neubig M, Ulrich D, Huguenard J (1998) Dendritic low-threshold calcium currents in thalamic relay cells. J Neurosci 18:3574–3588.

Destexhe A, Rudolph M, Fellous J-M, Sejnowski TJ (2001) Fluctuating synaptic conductances recreate in vivo-like activity in neocortical neurons. Neuroscience 107:13–24.

Douglas RJ, Martin KA, Whitteridge D (1991) An intracellular analysis of the visual responses of neurones in cat visual cortex. J Physiol (Lond) 440:659–696.

French CR, Sah P, Buckett KJ, Gage PW (1990) A voltage-dependent persistent sodium current in mammalian hippocampal neurons. J Gen Physiol 95:1139–1157.

Golding NL, Spruston N (1998) Dendritic sodium spikes are variable triggers of axonal action potentials in hippocampal CA1 pyramidal neurons. Neuron 21:1189–1200.

Golding NL, Staff NP, Spruston N (2002) Dendritic spikes as a mechanism for cooperative long-term potentiation. Nature 418:326–331.

Häusser M, Spruston N, Stuart GJ (2000) Diversity and dynamics of dendritic signaling. Science 290:739–744.

Hines ML, Carnevale NT (1997) The NEURON simulation environment. Neural Comput 9:1179–1209.

Hodgkin AL, Huxley AF (1952) A quantitative description of membrane current and its application to conduction and excitation in nerve. J Physiol (Lond) 117:500–544.

Holmes WR, Woody CD (1989) Effects of uniform and non-uniform synaptic "activation-distributions" on the cable properties of modeled cortical pyramidal neurons. Brain Res 505:12–22.

Huguenard JR, Hamill OP, Prince DA (1988) Developmental changes in Na^{+} conductances in rat neocortical neurons: appearance of a slowly inactivating component. J Neurophysiol 59:778–795.

Johnston D, Magee JC, Colbert CM, Christie BR (1996) Active properties of neuronal dendrites. Annu Rev Neurosci 19:165–186.

Koch C (1999) Biophysics of computation. Oxford: Oxford UP.

Larkman AU (1991) Dendritic morphology of pyramidal neurones of the visual cortex of the rat. III. Spine distributions. J Comp Neurol 306:332–343.

Larkum ME, Kaiser KM, Sakmann B (1999a) Calcium electrogenesis in distal apical dendrites of layer 5 pyramidal cells at a critical frequency of back-propagating action potentials. Proc Natl Acad Sci USA 96:14600–14604.

Larkum ME, Zhu JJ, Sakmann B (1999b) A new cellular mechanism for coupling inputs arriving at different cortical layers. Nature 398:338–341.

Llinás RR (1975) Electroresponsive properties of dendrites in central neurons. Adv Neurol 12:1–13.

London M, Segev I (2001) Synaptic scaling in vitro and in vivo. Nat Neurosci 4:853–855.

London M, Schreibman A, Häusser M, Larkum ME, Segev I (2002) The information efficacy of a synapse. Nat Neurosci 5:332–340.

Magee JC (2000) Dendritic integration of excitatory synaptic input. Nat Rev Neurosci 1:181–190.

Magee JC, Cook EP (2000) Somatic EPSP amplitude is independent of synapse location in hippocampal pyramidal neurons. Nat Neurosci 3:895–903.

Magee JC, Johnston D (1995) Characterization of single voltage-gated sodium and calcium channels in the apical dendrites of rat CA1 pyramidal neurons. J Physiol (Lond) 487:67–90.

Mainen ZF, Joerges J, Huguenard JR, Sejnowski TJ (1995) A model of spike initiation in neocortical pyramidal neurons. Neuron 15:1427–1439.

Matsumura M, Cope T, Fetz EE (1988) Sustained excitatory synaptic input to motor cortex neurons in awake animals revealed by intracellular recording of membrane potentials. Exp Brain Res 70:463–469.

McCormick DA (1992) Neurotransmitter actions in the thalamus and cerebral cortex and their role in neuromodulation of thalamocortical activity. Prog Neurobiol 39:337–388.

McCormick DA, Huguenard JR (1992) A model of the electrophysiological properties of thalamocortical relay neurons. J Neurophysiol 68:1384–1400.

Mel BW (1994) Information processing in dendritic trees. Neural Comput 6:1031–1085.

Migliore M, Hoffman DA, Magee JC, Johnston D (1999) Role of an A-type K^{+} conductance in the back-propagation of action potentials in the dendrites of hippocampal pyramidal neurons. J Comput Neurosci 7:5–15.

Paré D, Lang EJ, Destexhe A (1998a) Inhibitory control of somatic and dendritic sodium spikes in neocortical pyramidal neurons in vivo: an intracellular and computational study. Neuroscience 84:377–402.

Paré D, Shink E, Gaudreau H, Destexhe A, Lang EJ (1998b) Impact of spontaneous synaptic activity on the resting properties of cat neocortical pyramidal neurons in vivo. J Neurophysiol 79: 1450–1460.

Pouille F, Scanziani M (2001) Enforcement of temporal fidelity in pyramidal cells by somatic feed-forward inhibition. Science 293:1159–1163.

Rapp M, Yarom Y, Segev I (1992) The impact of parallel fiber background activity on the cable properties of cerebellar purkinje cells. Neural Comput 4:518–533.

Regehr W, Kehoe JS, Ascher P, Armstrong C (1993) Synaptically triggered action potentials in dendrites. Neuron 11:145–151.

Rhodes PA, Llinás RR (2001) Apical tuft input efficacy in layer 5 pyramidal cells from rat visual cortex. J Physiol (Lond) 536:167–187.

Rudolph M, Hô N, Destexhe A (2001) Synaptic background activity affects the dynamics of dendritic integration in model neocortical pyramidal neurons. In: Computational neuroscience: trends in research 2001 (Bower JM, ed), Neurocomputing, Vol 38, pp 327–333. Amsterdam: Elsevier.

Schwindt PC, Crill WE (1997) Local and propagated dendritic action potentials evoked by glutamate iontophoresis on rat neocortical pyramidal neurons. J Neurophysiol 77:2466–2483.

Schwindt PC, Crill WE (1998) Synaptically evoked dendritic action potentials in rat neocortical pyramidal neurons. J Neurophysiol 79:2432–2446.

Segev I, Rinzel J, Shepherd GM (1995) The theoretical foundation of dendritic function: selected papers of Wilfrid Rall with commentaries. Cambridge, MA: MIT.

Spencer WA, Kandel ER (1961) Electrophysiology of hippocampal neurons. IV. Fast pre-potentials. J Neurophysiol 24:272–285.

Spruston N, Jonas P, Sakmann B (1995) Dendritic glutamate receptor channels in rat hippocampal CA3 and CA1 pyramidal neurons. J Physiol (Lond) 482:325–352.

Steriade M, Timofeev I, Grenier F (2001) Natural waking and sleep states: a view from inside neocortical neurons. J Neurophysiol 85:1969–1985.

Stuart GJ, Häusser M (2001) Dendritic coincidence detection of EPSPs and action potentials. Nat Neurosci 4:63–71.

Stuart GJ, Sakmann B (1994) Active propagation of somatic action potentials into neocortical pyramidal cell dendrites. Nature 367:69–72.

Stuart GJ, Sakmann B (1995) Amplification of EPSPs by axosomatic sodium channels in neocortical pyramidal neurons. Neuron 15:1065–1076.

Stuart GJ, Spruston N (1998) Determinants of voltage attenuation in neocortical pyramidal neuron dendrites. J Neurosci 18:3501–3510.

Stuart GJ, Schiller J, Sakmann B (1997a) Action potential initiation and propagation in rat neocortical pyramidal neurons. J Physiol (Lond) 505:617–632.

Stuart GJ, Spruston N, Sakmann B, Häusser M (1997b) Action potential initiation and backpropagation in neurons of the mammalian CNS. Trends Neurosci 20:125–131.

Stuart GJ, Spruston N, Häusser M (2000) Dendrites. Cambridge, MA: MIT.

Svoboda K, Denk W, Kleinfeld D, Tank DW (1997) In vivo dendritic calcium dynamics in neocortical pyramidal neurons. Nature 385:161–165.

Traub RD, Miles R (1991) Neuronal networks of the hippocampus. Cambridge, MA: Cambridge UP.

Vaadia E, Haalman I, Abeles M, Bergman H, Prut Y, Slovin H, Aertsen A (1995) Dynamics of neuronal interactions in monkey cortex in relation to behavioural events. Nature 373:515–518.

Vetter P, Roth A, Häusser M (2001) Propagation of action potentials in dendrites depends on dendritic morphology. J Neurophysiol 85:926–937.

White EL (1989) Cortical circuits. Boston, MA: Birkhauser.

Williams SR, Stuart GJ (2000a) Site independence of EPSP time course is mediated by dendritic I(h) in neocortical pyramidal neurons. J Neurophysiol 83:3177–3182.

Williams SR, Stuart GJ (2000b) Action potential backpropagation and somato-dendritic distribution of ion channels in thalamocortical neurons. J Neurosci 20:1307–1317.

Williams SR, Stuart GJ (2002) Dependence of EPSP efficacy on synapse location in neocortical pyramidal neurons. Science 295:1907–1910.

Wong RK, Prince DA, Basbaum AI (1979) Intradendritic recordings from hippocampal neurons. Proc Natl Acad Sci USA 76:986–990.

Yamada WM, Koch C, Adams PR (1989) Multiple channels and calcium dynamics. In: Methods in neuronal modeling, Ed 2 (Koch C, Segev I, eds), pp 137–170. Cambridge, MA: MIT.

Yuste R, Tank DW (1996) Dendritic integration in mammalian neurons, a century after Cajal. Neuron 16:701–716.

Zhang S, Trussell LO (1994) Voltage clamp analysis of excitatory synaptic transmission in the avian nucleus magnocellularis. J Physiol (Lond) 480:123–136.

Zohary E, Shadlen MN, Newsome WT (1994) Correlated neuronal discharge rate and its implications for psychophysical performance. Nature 370:140–143.